Biologically-inspired Visible and Infrared Camera Technology Development

Elmer (Al) Williams[1]
Senior Electronics Engineer
alwilliams@engr.psu.edu

Michael A. Pusateri, Ph. D.[1]
Director, Senior Research Associate
mpusateri@engr.psu.edu

Jesse Scott[2]
Electrical and Computer Engineer
jesse.scott@heatinc.com

[1]Integrated Design Services
www.ecs.psu.edu/design/
Penn State University
149 Hammond Building
University Park, Pennsylvania 16802

[2]Digital Imaging Group
www.heatinc.com
heatfusion
10416 Theodore Green Boulevard
White Plains, Maryland 20695

Abstract- **Visible band and Infrared (IR) band camera and vision system development has been inspired by the human and animal vision systems. This paper will discuss the development of the Electro-Optical/Infrared (EO/IR) spectrum cameras from the front end optics, the detector or photon to electron convertor, preprocessing such as non-uniformity correction, automatic gain control, foveal vision processing done by the human eye, the gimbal system (human or animal eye ball and head motion), and the analog and digital paths of the data (optic nerve in humans). The computer vision algorithms (human or animal brain vision processing) will not be discussed in this paper. The Integrated Design Services in the College of Engineering at Penn State University has been developing EO/IR camera and sensor based computer vision systems for several years and combined with more than twenty years of developing imaging sensor stabilized platforms will use this imaging system development expertise to describe how the human and animal vision systems inspired the design and development of the computer based vision system. This paper will illustrate a block diagram of both the human eye and a typical EO/IR camera while comparing the two imaging systems.**

I. INTRODUCTION - HUMAN VISION AND EO/IR CAMERA VISION

The Penn State University (PSU) Integrated Design Services (IDS) has been developing image fusion algorithms for Night Vision Goggles (NVG) for the Army Night Vision Laboratory through a contract with Harsh Environment Applied Technology (HEAT) for the past three years. Several papers have been published at the 2008 and 2009 AIPR Conference on the image enhancement algorithms for NVG. PSU IDS has also been supporting the US Naval Research Laboratory (NRL) more than twenty years with the development of inertially stabilized platforms for EO/IR cameras [15][16][17]. This paper compares the development of EO/IR camera sensors to human sensors (eye) considering subsystem designs such as the optics, the detector, preprocessing such as non-uniformity correction (NUC) and Automatic Gain Control (AGC), the gimbal system or eyeball for the human sensor, and the output of the image data to the computer vision processor or brain for human vision. None of the authors of this paper are medical doctors; therefore we will be concentrating on the EO/IR camera development based on our understanding of the human eye sensor from knowledge gained from the references both online and written listed at the end of this paper [5][11][12][13][14][18].

To make a fair comparison we will be restricting the human sensor system to the right eye with no movement of the three degrees of freedom human neck as shown in Figure 1. We will be comparing only the sensor from both human and computer systems and not the image understanding processor (brain or computer).

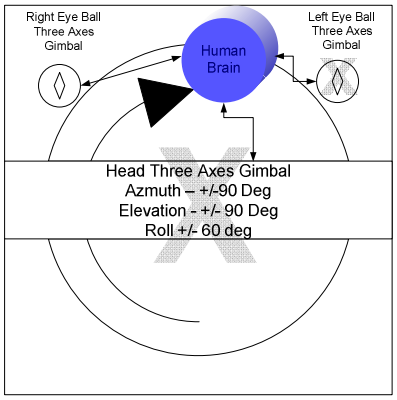

Figure 1: Human Vision High Level Block Diagram

A block diagram of the human vision system is shown in Figure 2. The block diagram for a typical EO/IR camera is shown in Figure 3. We will be referring to these two block

diagrams for the remainder of this paper as we compare the subsystems of both human and computer vision sensors.

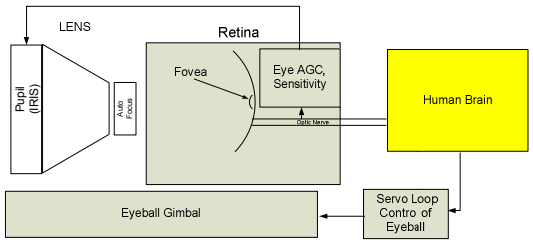

Figure 2: Human Vision Block Diagram

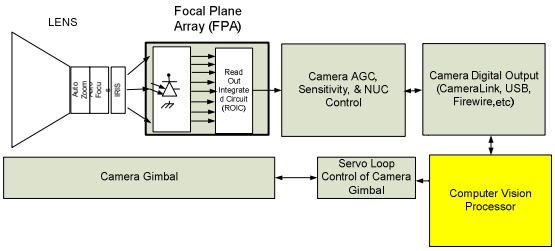

Figure 3: EO/IR Camera Block Diagram

For the human vision and EO/IR camera block diagram, the sensor subsystems have either a grey or white (the optics) background. The main central processor (brain or computer vision processor) has a yellow background. This paper is focused on the sensor, processing done inside the sensor, and the interface from sensor to main vision processor. We will not focus on the human brain or computer vision processor (yellow background in block diagrams.) Notice that the gimbal (eyeball for human sensor) and servo loop are part of the sensor in the block diagrams. The position of the IRIS control is located in the front of the lens (the pupil) for the human eye lens and is in the back of the lens for the EO/IR camera vision system. The lens in both systems have a auto focus control but only the EO/IR camera has auto zoom. The human vision system has no need for auto zoom due to the foveal processing done in the human vision system. Details of foveal process will be described later. The retina (photon to neuron convertor) is curved in the human eye verses the Focal Plane Array (FPA) detector in the computer vision sensor is flat. The flat detector causes some distortion issues that must be corrected by the computer vision processor. The final difference between the two sensors is the Automatic Gain Control (AGC) which is done by a digital feedback from the computer vision processor verses the AGC done in the eye by the pupil and the ganglion cells in the retina. We will now describe the details of the five subsystems mentioned earlier for the human sensor and the EO/IR computer vision sensor and identify the advantages and disadvantages of the parameters of each sensor.

II. THE HUMAN AND CAMERA OPTICS COMPARISON

A comparison of the optics for the human eye and a typical EO/IR camera lens is shown in Figure 4. The first parameter compared is the Field of View (FOV) which is 180 by 140 degrees for the human eye and 40 by 30 degrees for a typical EO/IR camera or sensor that could be used in applications such as night vision goggles. EO/IR cameras would like to use a lens that would provide a larger FOV; however, distortion is an issue resulting from flat FPAs. Also, FPAs have a much smaller pixel counts compared to the human eye resulting in a larger Instantaneous FOV (IFOV) causing fewer pixels on a target at long range. EO/IR cameras have an advantage in spectral range with the availability of Ultra-Violet (UV), visible, Near IR (NIR), Short Wave IR (SWIR), Mid Wave IR (MWIR), and Long Wave IR (LWIR) covering a spectral bandwidth of .3 to 12 micrometers. The spectral range of the human eye is limited to the visible band (0.4 to 0.7 micrometers.)

Parameter	Human Eye	EO/IR Camera
Field of View (FOV)	180 by 140 degrees	40 by 30 degrees
Spectral Range	.4 to .7 um	.3 to 12 um
Distortion	Very little due to curved retina	At 120 degrees or greater distortion has an overwhelming effect on image quality
Auto Focus	The refractive lens can change shape to produce a sharp ("in focus") image	Need feedback from Vision processor to auto focus on part of the image
Auto Zoom	Eye does not need to zoom due to fovea	90X Zoom lens needed to match human eye
Auto Iris	This provides a focal-ratio for the eye in the range f/3 to f/8 (approximately)	Auto IRIS available from f/1.2 to f/22, but long time constant
Weight	28 grams (.98 Ounces)	115 grams (3.45 Ounces)

Figure 4: Human Eye and Camera Optics Comparison

Figure 5 shows the UV to LWIR part of the electromagnetic spectrum with the bandwidth of each sub band in micrometers.

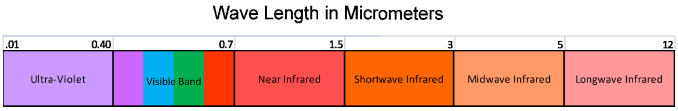

Figure 5: Electromagnetic Spectrum from Ultra-Violet to Long Wave Infrared

There is very little distortion in the human eye with a wide FOV lens due to the curved retina detector at the back side of the lens. Distortion is a huge issue for EO/IR sensors as the FOV increases above 80 degrees. Typical night vision goggles provide a 40 by 30 degree FOV. A more desirable FOV would be 120 by 50 degrees. This wider FOV presents

two problems with currently available detector arrays. The first problem is the distortion issue caused by the flat FPA behind a wide FOV lens. The second problem arises because most FPAs are designed with a four (horizontal axis) to three (vertical axis) aspect ratio. Figure 6 illustrates the distortion issue with EO/IR cameras using wide FOV lenses. The top image in Figure 6 was taken from a MWIR camera with a 120 by 17 degree FOV anamorphic lens used by the NRL Gunfire Detection and Location System [1]. The middle image is a visible spectrum color mosaic of the same scene. It should be noted that the anamorphic lens still covers a wider field of regard than the color mosaic. The bottom image is a direct mapping of known pixel location in the MWIR camera image (top image) to the pixel location of the middle visible band image for a subset of data points. An estimation technique was used to generate a look up table for the rest of the pixel locations (on the order of 80,000).

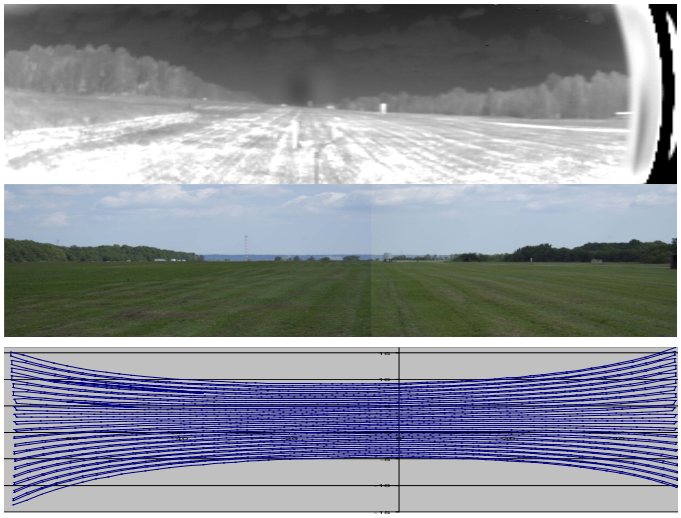

Figure 6: Distortion in Wide Field of View Optics Due to Flat Detector

The human eye does auto focus using the refractive lens that can change shape to produce a sharp ("in focus") image in a young person. As humans get older the focus motor no longer functions accurately and the need for glasses is required to help focus on near or far objects. EO/IR cameras also have an auto focus capability. Usually the sensor processor (AGC, NUC subsystem in Figure 3) looks at the image produced by the FPA and moves the focus lenses inside the optical lens to keep the image in focus. Another more flexible approach to auto focus is to allow the user of the computer vision system to focus on a particular object in the FOV using the computer vision processor. Allowing the user to select the object or region in the image to auto focus also provides feedback to the sensor for adjusting the gain or contrast of the imagery.

Auto Zoom is not needed in the human eye and is required by the EO/IR camera system that is using only one camera for wide FOV and narrow FOV vision processing. A 20X zoom lens is required for 40 degrees down to 2 degrees for night vision applications. To match the human eye 180 degree FOV with the capability to steer the 2 degree fovea would require a 90X zoom lens for the EO/IR camera.

Both the human and EO/IR camera based vision systems provide auto IRIS control. The human eye provides a focal ratio in the range of f/3 to f/8 by adjusting the pupil at the front of the lens in Figure 2. The f/# is equal to the focal length divided by the aperture. Under low light conditions at night the eye would open the aperture or pupil up (f/3) to allow more photons into the fixed focal length lens. In bright sunlight conditions the eye would close the pupil moving towards an f/8 optical system. EO/IR camera lenses have auto Iris capability with typical aperture range of f/1.2 to f/22. Again during low light conditions the auto IRIS should move towards f/1.2 to allow more photons into the camera detector and closing the aperture towards f/22 during bright sunlight conditions.

The human eye sensor including the gimbal (eyeball) weighs 28 grams or .98 ounces. The weight of a typical visible band camera with a small lens (large f/#) is 115 grams or 3.45 ounces not including the gimbal! The human vision sensor has a tremendous weight advantage over currently available EO/IR camera technology. Also, the IR cameras currently available are much larger and heavier than visible band cameras.

III. RETINA (PHOTON TO NEURON) AND THE DETECTOR (PHOTON TO ELECTRON) CONVERTOR

As mentioned in the earlier sections of this paper, the human eye uses the retina with many of the pixels concentrated in the fovea to eliminate the need for auto zooming. A distribution of the pixels or rods and cones in the right eye of a human is illustrated in Figure 7. In doing a literature search for how the rods and cones are distributed, almost all of the references were based on a 1935 paper written by a Danish Scientist G. A. Osterberg [2]. Figure 7 is a plot of the data very carefully collected by Dr. Osterberg in 1935 based on dissecting the right eye of a 16 year old boy who lost sight from the eye due to a severe lesion. From Dr. Osterberg's notes, "The retina was found to be non-detached and perfectly sound." Dr. Osterberg plotted the rods and cones distribution based on the distance from the fovea in millimeters. We chose to re-plot the data based on the angle in degrees from the fovea. The X-axis is a non linear plot of the angle in degrees from the fovea centered at zero degrees. The middle two degrees is expanded to show the density of cones in this area. Since this is a view of the right eye looking out to the world, the angle increases to the left of the fovea to 94.6 degrees where the nose blocks human vision.

The angle increases to the right of the fovea to 74.5 degrees where the temple blocks the human vision. The blind spot due to the optic nerve intersection with the retina occurs at

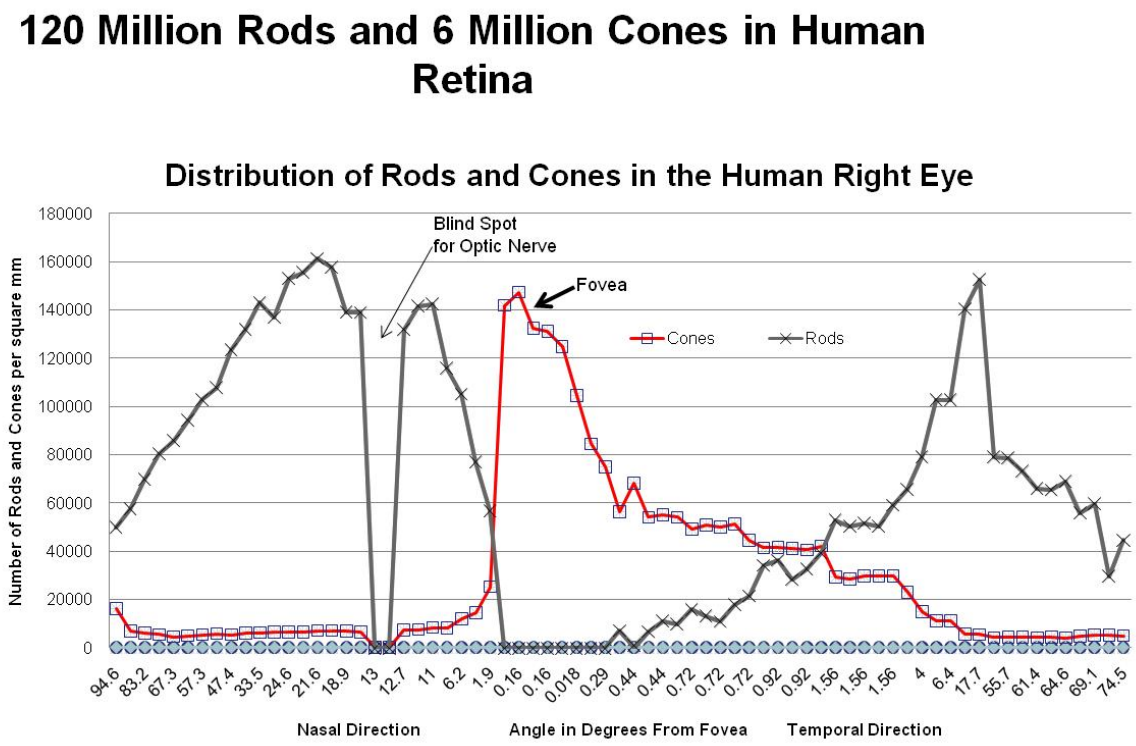

Figure 7: Distribution of Rods and Cones in the Human Right Eye

approximately 13 degrees in the nasal direction for the right eye.

Humans do not see this blind spot due to the brain "filling in" the missing pixels from the other eye. Notice that almost all of the approximately six million cones are located in the fovea while very little of the rods are in the fovea. The rods that are responsible for night and peripheral vision are almost nonexistent in the fovea. Rod density rises to a peek at approximately twenty degrees on both sides of the fovea and then drops linearly in both directions from 20 degrees to 90 degrees from the fovea. Notice that the plot of angle in degrees from the fovea is non linear in both directions all the way out to 90 degrees. Since this is a plot of the actual density samples collected, the nasal verses temporal density curves appear different at first glance. Looking closer at the non linear plot shows the curves of the density are very similar on both sides of the fovea.

Figure 8 is a table showing the currently available FPA sizes for EO/IR cameras covering the visible to LWIR spectral bands. The array sizes in the table are for available products and not one of a kind prototypes. Also, all the array sizes are for uncooled arrays that could be used in a small light weight package and are low power without cryo-cooler requirements. The human eye retina with 110 million rods and 6 million cones is listed in the table to show the huge advantage the human sensor has compared to the visible band array size of 2048 (H) by 2048 (V).

Spectral Band	Array Size
Visible Near IR (.4 to .7 um)	2048 (H) by 2048 (V)
Short Wave IR (1.0 to 2.5 um)	640 (H) by 512 (V)
Mid Wave IR (3 to 5 um)	64 element Linear Array
Long Wave IR (8 to 12 um)	1024 (H) by 768 (V)
Human Retina	110M Rods & 6M Cones

Figure 8: EO/IR Camera FPA Compared to Human Retina Pixel Resolution

Figure 9 illustrates a night time scene of a person walking on a dirt road from three IR cameras with a 40 degree FOV. The three cameras are operating in LWIR (top left), VisNIR (bottom left), and SWIR (bottom right). The imagery was collected from a multi-camera and multi-spectral video library platform [3]. The 40 degree FOV is the current FOV for sensors used in night vision goggles. The top right quadrant in Figure 9 is a table of Metadata collected synchronously with the three band imagery [3].

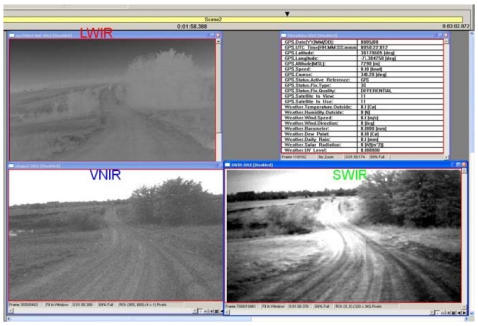

Figure 9: Multiband Imagery from IR Cameras with 40 Degree FOV

IV. AUTOMATIC GAIN CONTROL (AGC)

Figure 10 illustrates a typical AGC of a sensor by the image processor using a digital feedback loop. The AGC loop between the sensor and the image processor is a course gain control. The function of course gain control is to keep the sensor's digital intensity values matched to the input of the image processor and within the dynamic range of the A/D converter of the sensor.

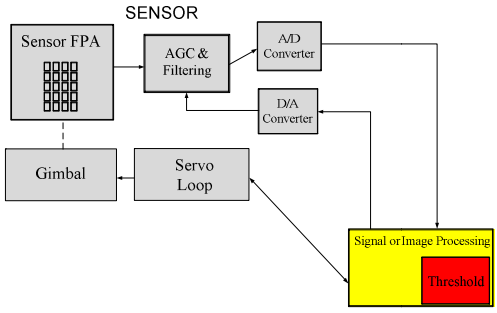

Figure 10: Automatic Gain Control in an EO/IR Camera

Figure 11 is an image from the NRL multiband linear array imager [4] while looking directly into the sun. The imagery is saturated in all bands and illustrates the problem of tracking targets that are above or below the dynamic range of the A/D converter. Figure 12 is an algorithm for course gain control used to keep the maximum and minimum intensity values from the sensor away from the top and bottom rails of the sensor A/D converter. Notice the threshold parameter in red in the image processor in Figure 10. Changing the AGC values in the sensor has a direct impact on the threshold value for identifying targets from the background. Changing the course gain using the AGC in the sensor without changing the threshold value could raise the false alarm rate or lower the target detection rate of the image understanding system.

The concept of AGC (course gain only) used by typical EO/IR cameras was described in this section. We will now compare human and computer vision AGC. In both the human and computer vision systems, the course gain is adjusted using a combination of the IRIS control and the integration time in the detector.

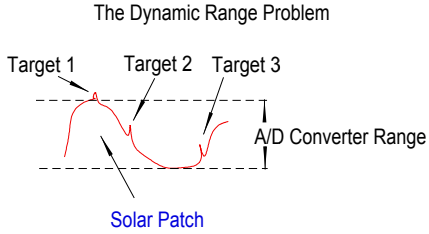

Figure 11: The Dynamic Range Problem

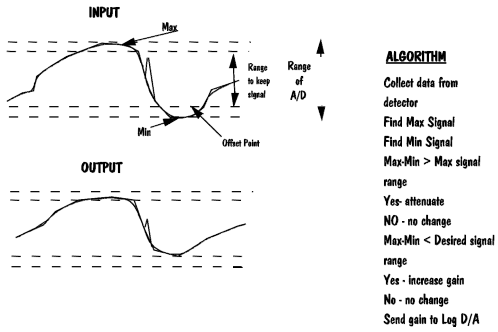

Figure 12: Course Gain Algorithm

Refering to Figure 4, the auto IRIS parameter for both the human and computer vision sensor were compared. The human IRIS can adjust the focal-ratio from f/3 (largest diameter of the aperature) to f/8 (smallest aperature diameter). A typical EO/IR camera IRIS range is from f/1.2 to f/22. Both auto IRIS adjustments are done with a motor control to open or close the aperture. For both sensors, it takes approximately 20 seconds for the auto IRIS motor to change the aperture diameter from wide open (small f/#) to the smallest diameter (large f/#).

The integration time for the human retina is controlled by the ganglion cells and will adjust integration time from 100 milliseconds (lowest sensitivity) to 200 milliseconds (highest sensitivity or full dark adaptation). However, it takes about 20 minutes to change from the highest to the lowest sensitivity.

Integration time in EO/IR camera sensors is accomplished in the readout integrated circuit (ROIC) (Figure 3). Typical

integration times for FPAs and ROICs vary from 1 to 15 milliseconds (depending on the material used in the FPA) for lowest sensitivity to hundreds of milliseconds for high sensitivity. Using a smart AGC algorithm in the image processing computer (see Figure 10), the integration time can be changed as rapidly as once per frame. At 60 frames per second, the integration time could be changed every 16.6 milliseconds. The computer vision system AGC can be changed much more rapidly than the human vision AGC which relies on the IRIS control (on the order of several seconds) for course gain control and hence the computer vision AGC or course gain control has a significant advantage.

V. THE SENSOR GIMBAL

To move a sensor very rapidly from point A to point B with little or no overshoot when approaching point B requires a motor with high torque. The definition of the moment of inertia (J) is a measure of the ability of a rotating mass to accelerate when driven by an applied torque. The moment of inertia depends not only upon the gimbal and payload mass but also upon the spatial distribution of the mass. It is a corollary to Newton's (F=ma) formula for rotating masses expressing a relationship between Torque (T) exerted on a rotating body and the resultant rotational acceleration (α) of the mass.

This relationship can be expressed mathematically as:

$$J = T / \alpha$$

Where: J = Moment of inertia in units of (oz. in.sec ^{2}/rad)
= Moment of inertia in units of (Newton*meter*sec^2 /rad)
T = Applied torque in (oz.in.)
= Applied torque in (Newton*met)
α = Angular acceleration in (radians/sec ^{2})

In order to move the fovea around the FOV of the human retina and fixate the fovea on a target in the shortest time possible requires a gimbal motor that provides high acceleration and hence high torque. Figure 13 shows the human eyeball with the six muscles used to provide the torque and high acceleration for the three degrees of freedom required to move the fovea within the FOV of the human retina [5]. The strongest muscles in the human body are the six muscles used for eye motion and provide the high torque required for high acceleration.

Figure 14 is a picture of a gimbal with a payload consisting of multiple EO/IR cameras. The gimbal and the servo loop shown in Figure 15 were developed by the Naval Research Lab (NRL) [4] and Penn State University. Notice the equation for torque (T(s) = Jά(s)) over the motor in the servo loop equation. Obtaining high torque in a gimbal system with a payload, while keeping the motor size and weight low, requires the use of rare earth materials for the magnets which increases the cost of the motor. The 28 gram high torque human eyeball has a huge advantage over the equivalent big expensive EO/IR sensor and gimbal. A typical small visible band camera weights 115 grams and does not include the weight of the gimbal.

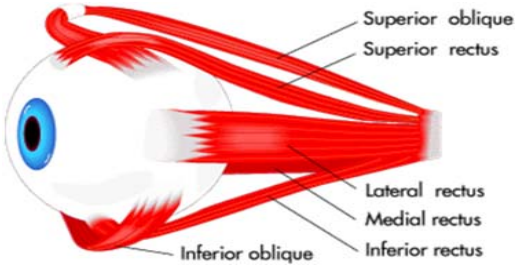

Figure 13: Human Eyeball Gimbal

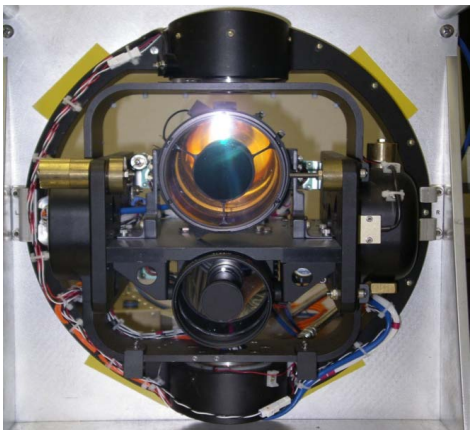

Figure 14: Multi-Camera Gimbal

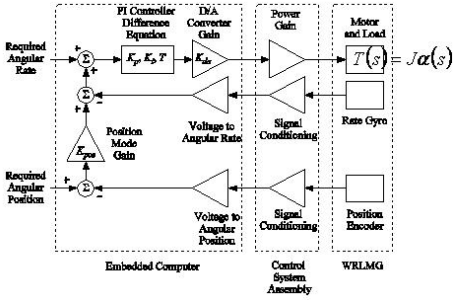

Figure 15: Servo Loop for Camera Gimbal

VI. HUMAN EYE FOVEA VISION

The human Eye has 180 degree horizontal by 140 degree vertical with 1 to 2 degree Field of View (FOV) in the Fovea area. The eyeball gimbal is capable of scanning over the entire 180 by 140 Field of Regard (FOR) of the retina. The strong high torque muscles in the human eye provide the acceleration required to move the fovea around the 180 by 140 degree FOR of the human retina and fixate the fovea on a target in the shortest time. Figure 16 consists of two targets with four different color circles that are numbered.

Figure 16: Tracking with Fovea in Human Retina

Fixating the fovea on the target on the left allows you to read the numbers and identify the colors of the circles. The target on the right is outside the fovea and you can use your peripheral vision to sense that an object is to the right. These two targets were used to count the number of times over a 10 second period that a human could fixate on one of the targets and then move and fixate on the other target. A timer was set for 10 seconds while the eye was moved from the target on the left and then moving the fovea to the target on the right. After centering the target in the fovea and fixating long enough to recognize the numbers in the circles, the fovea was moved to the other target. I was able to fixate on the targets 12 times in 10 seconds. This experiment gives a good indication of how good the eyeball is at accelerating away from one target and then decelerating as you approach the other target. EO/IR sensor gimbals use a similar experiment to measure the functionality of the gimbal and servo loop. The small 28 gram eyeball does a much better job of using fovea processing to track multiple targets in the FOR of the retina compared to the EO/IR sensor.

VII. THE ANALOG AND DIGITAL PATHS OF THE DATA (OPTIC NERVE IN HUMANS)

Table 1: Typical Illuminance of Day and Night Conditions

Illuminance	Background Conditions
.00010 Lux	Starlight Clear Night
0.01 Lux	Quarter moonlight
0.27 Lux	Full Moon Clear Night
50 Lux	Family Living Room
100 Lux	Very dark overcast day
32,000-130,000 Lux	Direct Sunlight

Imagery is passed from the retina to the brain over two analog data paths in the optic nerve. One analog path passes the data from the 110 M rods in the178 Degree FOV outside of fovea. The other analog path passes the data from the 6 M cones in the 2 Degree Fovea. Feedback from the brain to the eye gimbal control points the fovea at the desired target.

Table 1 lists the illuminance in Lux for background conditions from starlight clear night to looking directly at the sun with a visible band sensor. Note that the illuminance difference is $1x10^9$. To pass the entire dynamic range for an illuminance difference of 1 x 10^9 would require 30 bits for each pixel in the image. To pass a 110M pixel image at 32 bits per pixel requires 440 MB per frame * 30 Frames per Second = 13.2 GB/sec. None of the existing digital protocols such as Gig-E, 10Gig-E, and CameraLink are capable of passing the imagery at this high data rate.

The sun black body curve in Figure 17 is an irradiance curve for the sun at 6000 degree centigrade which peaks in the visible band and rolls off exponentially as the wavelength moves out towards the longer wavelength bands. Due to this exponential decrease in irradiance as the wavelength of the incoming photons shifts towards the longer wavelength IR bands, the number of bits required to capture the entire dynamic range reduces. However, even dropping down to 16 bits would require a data path capable of passing 6.6 GB/sec. This rate is also too high for the existing digital protocols.

The human vision system uses a distributed processing network with the front end processing done in the retina combined with the human brain processing of data from two data paths in the optic nerve. Most EO/IR camera based vision systems attempt to pass the entire dynamic range (30 bits per pixel) to the central processor. The computer vision system must take advantage of preprocessing at or near the FPA to reduce the number of bits per pixel passed over a high speed data path to the central processor (similar to human vision systems).

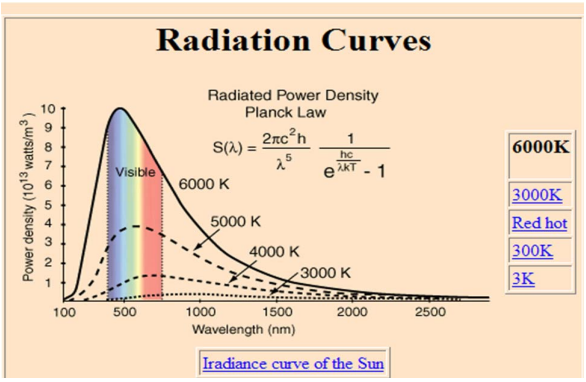

Figure 17: Sun Black Body Curve

VIII. CONCLUSIONS

EO/IR camera based computer vision systems provide a greater spectral range compared to the human eye based vision system. EO/IR cameras also have a better AGC compared to the human eye.

The human eye and brain have an advantage over manmade computer vision systems in regards to all the other parameters discussed in the paper (optics, detector density, distribution of pixels, gimbal system, foveal vision processing, and the distributed image processing system that reduces the data rate of the imagery between the eye sensor and the brain).

Figure 18 is a diagram of a vision system that takes advantage of the good attributes of both the human and computer vision system. The multispectral EO/IR sensors with a smart AGC algorithm in the FPGA based computer would be used to pass the EO/IR imagery to a display with the use of an eye tracker such as the one developed by Rochester Institute of Technology (RIT) that was demonstrated during the poster paper session at the AIPR 2009 Workshop [7] [8][9][10]. The eye tracker would then feedback the location of the foveal in the FOV of the multispectral imagery to the FPGA based vision processor. The FPGA processor could then feedback information to the detector and the optics to: adjust the depth of view, focus on a particular object in the FOV, zoom in on the object of interest, adjust the AGC of the imagery based on a region of interest around the target, etc. All of this feedback could be done with minimal latency since the human operator is only required to fixate the fovea on the target of interest.

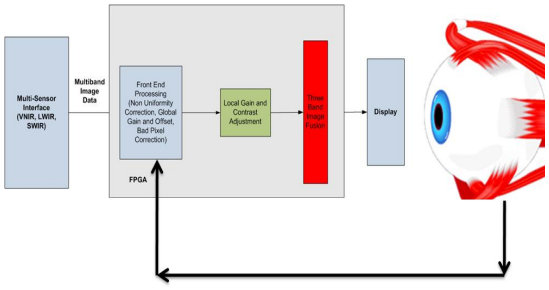

Figure 18: EO/IR Camera Computer Vision with Feedback from Human Eye

IX. REFERENCES

[1] Price, J.; Maraviglia, C.; Seisler, W.; Williams, E.; Pauli, M. "System Capabilities, Requirements and Design of the GDL Gunfire Detection and Location System", 33nd Applied Imagery Pattern Recognition Workshop, 2004.

[2] Osterberg, G. A. "Topography of the Layer of Rods and Cones in the Human Retina." 1935.

[3] Williams, E.; Pusateri, M. A.; Siviter, D. "Multicamera-Multispectral Video Library – An Algorithm Development Tool", 37th Applied Imagery Pattern Recognition Workshop, 2008.

[4] Michelizzi, M. et al, "Image Fusion with Multiband Linear Arrays", 37th Applied Imagery Pattern Recognition Workshop, 2008.

[5] Bianco, C. "How Vision Works" http://health.howstuffworks.com/eye.htm 21 October 2009.

[6] Nave, C. R. Department of Physics and Astronomy, Georgia State University, Email: RodNave@gsu.edu http://hyperphysics.phy-astr.gsu.edu/hbase/bbrc.html

[7] DeAngelus, M.; Pelz, J.B. "Top-down control of eye movements: Yarbus revisited." *Visual Cognition*, (3), 1-22, 2009.

[8] Munn, S.; Pelz, J. B. "3D Point-of-regard, position, and head orientation from a portable monocular video-based eye tracker" *Proc. of the* 2008 *ACM SIGCHI Eye Tracking Research & Applications Symposium*, Savannah, GA. 2008.

[9] Li, F; Munn, S.; Pelz, JB. "A model-based approach to video eye tracking" *Journal of Modern Optics* 55(4), 503-531. 2008.

[10] Pelz, J.B.; Rothkopf, C "Oculomotor behavior in natural and man-made environments" In R. VanGompel (Ed.), *Eye movements: A window on mind and brain*, Elsevier Press. 2007.

[11] DeValois, R.; DeValois, K. "Spatial Vision", Oxford University Press, 1988.

[12] Underwood, G. "Cognitive Processes in Eye Guidance", Oxford University Press, 2005.

[13] Wandell, B. "Foundations of Vision", Sinauer Associates, Inc. 1995.

[14] Albus, J. "Brains, Behavior, & Robotics, BYTE Books, 1981.

[15] Williams, E.F. et al "Optimization of a Gimbal Scanned IR Seeker," SPIE Conference on Aerospace Sensing, April 1991.

[16] Williams, E.F. et al "Infrared Sensor Data Fusion for Target Detection, Identification, and Tracking," SPIE conference on Aerospace Sensing Components and Systems, April 1990.

[17] Williams, E.F.; Evans, R.H.; Stockum, L. "Infrared Antiship-seeker Simulator," SPIE Acquisition, Tracking, and Pointing III, March 1989.

[18] Bradley, Arthur; Indiana University School of Optometry, "Physiological Optics II: Visual Function," http://www.opt.indiana.edu/v664/index.htm